Journal of Environmental Chemical Engineering 11 (2023) 110609

Contents lists available at ScienceDirect

Journal of Environmental Chemical Engineering

journal homepage: www.elsevier.com/locate/jece

Reflector design for the optimization of photoactivated processes in tubular reactors for water treatment

M. Martín-Sómer [a,b,c,*], J. Moreira [b,c,d], Carla Santos [b,c], Ana I. Gomes [b,c], J. Moreno-SanSegundo [e], Vítor J.P. Vilar [b,c,**], J. Marugán [a]

[a] Department of Chemical and Environmental Technology, ESCET, Universidad Rey Juan Carlos, C/Tulipán s/n, Móstoles, Madrid 28933, Spain
[b] LSRE-LCM – Laboratory of Separation and Reaction Engineering – Laboratory of Catalysis and Materials, Faculdade de Engenharia da Universidade do Porto, Rua Dr. Roberto Frias, 4200-465 Porto, Portugal
[c] ALiCE – Associate Laboratory in Chemical Engineering, Faculdade de Engenharia da Universidade do Porto, Rua Dr. Roberto Frias, 4200-465 Porto, Portugal
[d] Universidad Politécnica de Madrid (UPM), E.T.S de Ingenieros Industriales, Departamento de Ingeniería Química Industrial y del Medio Ambiente, C/José Gutiérrez Abascal 2, 28006 Madrid, Spain
[e] Escuela Técnica Superior de Ingeniería Informática, Universidad Rey Juan Carlos, C/Tulipán s/n, Móstoles, Madrid 28933, Spain

ARTICLE INFO

Editor: Despo Kassinos

Keywords:
Ray tracing simulation
Optical efficiency
Radiation optimization
Energy consumption
UV-based treatment
Advanced oxidation process

ABSTRACT

Photoactivated advanced oxidation processes have excellent performance in removing recalcitrant pollutants from water. However, the high operating cost associated with the energy consumption of UV lamps is a big drawback. In this work, the design and optimization of the reflector in a tube-in-tube membrane photoreactor were carried out using a ray tracing methodology to maximize the light deployed to the reactor. Simulations were carried out using different lamps/reactor arrangements with 1, 2 and 3-sided flat reflectors and with circular and parabolic geometries. Results showed that direct radiation is maximized when the distance reactor-lamps is minimized, increasing optical efficiency. On the other hand, it was observed that for the flat reflectors, the closer the furthest point of the reflector to the center of the reactor, the higher optical efficiency is achieved due to the reduction in the number of bouncing rays in the reflector. In the case of parabolic geometries, some additional considerations are necessary, since not only the distance at which the reflector is placed matters, but also its geometrical focus. The best performance is achieved for those in which the distance from the furthest point of the reflector to the center of the reactor was lower and the lamps placed near the focus of the parabola. For the studied reflector geometries, the calculated optical efficiencies when using anodized aluminum were 46.1%, 56.5%, 60.0%, 41.8%, and 65.9% for reflectors of 1, 2, and 3 sides, cylinder, and parabola, respectively. Model predictions were successfully validated using experimental ferrioxalate actinometry data, confirming the huge potential of this simple simulation methodology for photoreactor design purposes.

1. Introduction

Photoactivated advanced oxidation processes (AOPs), such as photocatalysis, photo-Fenton, UVC/H_2O_2, UVC/O_3, UVC/persulfate among others, generates reactive oxygen species able to be used for oxidation and reduction reactions in environmental remediation purposes, or even in organic synthesis. However, the main drawback is the high energy consumption associated with the generation of UV radiation [1,2]. Low-pressure mercury lamps have been traditionally used [3], although their electricity conversion efficiency into useful light is low. In recent years, LED technology has greatly developed, reaching high electrical efficiencies in the UVA range [4–6]. However, the efficiency of LED in the UVC range has not yet reached the level of development necessary, and their use is still less efficient than conventional mercury lamps. For this reason, it is vital to perform a correct design of the reactors where photoactivated processes are implemented to use most of the emitted photons in an efficient way.

When a low-pressure lamp with a cylindrical shape is used, the most

* Corresponding author at: Department of Chemical and Environmental Technology, ESCET, Universidad Rey Juan Carlos, C/Tulipán s/n, Móstoles, Madrid 28933, Spain.
** Corresponding author at: LSRE-LCM – Laboratory of Separation and Reaction Engineering – Laboratory of Catalysis and Materials, Faculdade de Engenharia da Universidade do Porto, Rua Dr. Roberto Frias, 4200-465 Porto, Portugal.
E-mail addresses: miguel.somer@urjc.es (M. Martín-Sómer), vilar@fe.up.pt (V.J.P. Vilar).

https://doi.org/10.1016/j.jece.2023.110609
Received 4 May 2023; Received in revised form 27 June 2023; Accepted 19 July 2023
Available online 21 July 2023

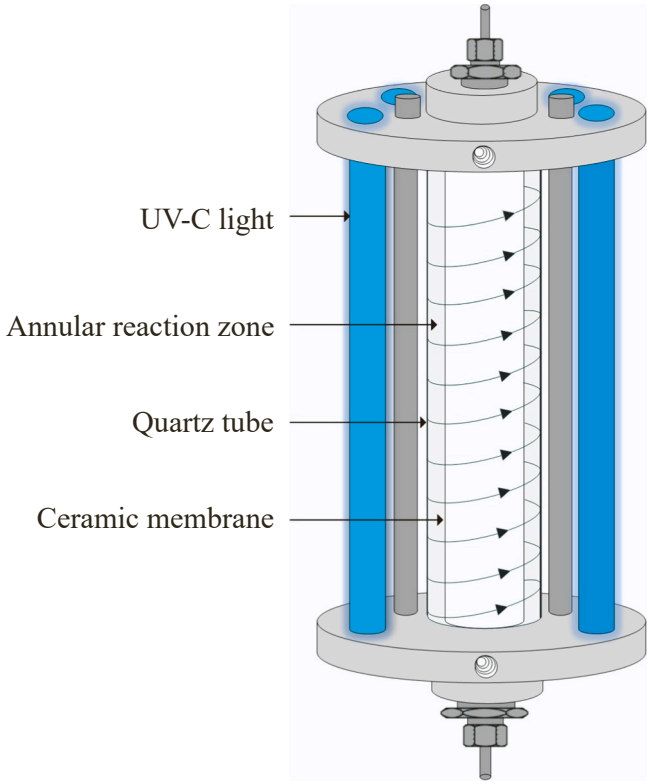

Fig. 1. Schematic representation of the tube-in-tube membrane photoreactor.

Table 1
Radiation emitted by the 4 lamps used in the tube-in-tube reactor.

	Radiation emission (W)
UVC lamp 1	1.3 ± 0.2
UVC lamp 2	1.59 ± 0.08
UVC lamp 3	1.6 ± 0.1
UVC lamp 4	1.34 ± 0.08

efficient configuration is placing the light source in the axis of an annular reactor. However, this arrangement is not always possible and external illumination is employed. In these cases, the use of reflectors is critical. Moreover, due to the unavoidable energy losses in the bounces of photons in non-ideal reflectors, their geometry must be carefully considered. The design of the reflectors needs to consider the path followed by the light once it leaves the lamp. Ray paths can be calculated using different numerical approaches, including Monte Carlo and finite volume methods [7,8]. Other more complex methods are based on computational fluid dynamics (CFD) software, either commercial [9–12] or open source [13,14]. The advantage of CFD methods is that they allow the coupling of the radiation modeling into multiphysics systems, including fluid dynamics, mass transfer, or chemical reaction. However, these methods require a high computational cost and calculation times [27,28], which is not practical in parametric studies for optimizing multiple variables. To overcome this limitation, in a recent work, our research group reported a new ray tracing tool based on Microsoft Excel for evaluating the concentration factors in compound parabolic collectors (CPC) reactors [15,16]. The main advantage of this tool is the speed of the calculations allowing the evaluation of a large number of parametric studies in a short time.

The main objective of this work was the optimization of the reflector design used in a tube-in-tube photoreactor in which 4 UVC mercury lamps were used as the light source. This type of reactor does not allow the location of the lamp in the inner annulus, as this space is occupied by a tubular membrane used to deliver oxidant (liquid or gas) or catalyst (ferrous iron) solutions, enabling a homogeneous radial and longitudinal distribution of the oxidant/catalyst in the reactor annulus [17–19]. For the implementation of this study, the ray tracing tool previously developed was adapted to allow calculations in reactors not only with solar lighting but also using cylindrical lamps as light sources. Different reflector geometries were studied, including 1, 2, and 3-sided flat reflectors, as well as circular and parabolic geometries. Materials with different reflectance were also evaluated. The results obtained in the simulations were experimentally validated with actinometric measurements.

2. Material and methods

2.1. Photoreactor setup

The optimization of the efficiency in the delivery of UVC photons was carried out in a tube-in-tube membrane reactor developed by Vilar et al. [19]. This tube-in-tube reactor consists of an inner ceramic ultrafiltration membrane (γ-Al_2O_3 membrane from Inopor GmbH) and an outer quartz tube (Fig. 1). The ultrafiltration membrane presented an outside diameter of 2.03 cm, an inside diameter of 1.55 cm, a total length of 20 cm, and an illuminated length of 17.4 cm. The pore size was 10 nm, while the porosity ranged between 30% and 55%. The quartz tube presented the following dimensions: outer diameter = 4.2 cm; thickness = 0.18 cm; total length = 20 cm; illuminated length = 17.4 cm. The reactor inlet and outlet are perpendicular to the flow direction, tangential to the quartz tube, in the horizontal plane and at the top on opposite sides, inducing a helical movement of the water around the membrane, as described elsewhere [19].

As the light source, four Philips TUV 11 W FAM/10X25BOX lamps were used with a peak emission centered at 254 nm. The lamps were arranged symmetrically around the reactor as shown in Fig. 1 at 3.3 cm from the center of the reactor. To improve the efficiency in the use of the emitted photons, the lamps were surrounded by anodized aluminum reflectors with different geometries. Details on the total and specular reflectance properties of the anodized aluminum can be found elsewhere [20].

An annular reactor was used for the sole purpose of characterizing the 4 UVC lamps used in the reactor described above. In this case, the lamp was located inside a quartz tube (outside diameter of 23.0 mm and thickness of 1.4 mm) in the axis of the annular reactor. The outer tube (length of 186.0 mm and inside diameter of 72.0 mm) is made of stainless steel [21]. The annular configuration ensures that all emitted photons reach the reaction zone, with the exception of those absorbed by the quartz tube. Therefore, results showed the exact amount of radiation emitted by each lamp, which was determined by actinometric measurements. The results obtained for each of the 4 lamps used in the tube-in-tube photoreactor are shown in Table 1.

2.2. Actinometric measurements

Actinometric measurements were carried out by circulating a ferrioxalate solution in the annular zone of the reactor, being able to determine the amount of radiation reaching the reaction zone in each studied configuration. The actinometric solution was prepared with distilled water, adding 2.27 g of $H_2C_2O_4{\cdot}2H_2O_2$ (final concentration of 18 mM oxalic acid), 1.47 g of $Fe_2(SO_4)_3{\cdot}5H_2O$ (final concentration of 6 mM Fe^{3+}) and 100 mL of H_2SO_4 1 N. The final volume of the solution was 1 L. The amount of ferrous ions formed during the irradiation period was monitored by the conversion to the colored tris-phenanthroline complex: 0.25 mL of sample was added to 2.5 mL of buffer (54.18 g of $C_2H_3NaO_2{\cdot}3H_20$ and 5 mL of 96% pure H_2SO_4 in 500 mL of water), 6.25 mL of H_2O, and 1 mL of phenanthroline (1 g/L solution), resulting in an orange-colored complex. The absorbance was measured at 510 nm using a VWR UV-6300PC spectrophotometer. The number of ferrous

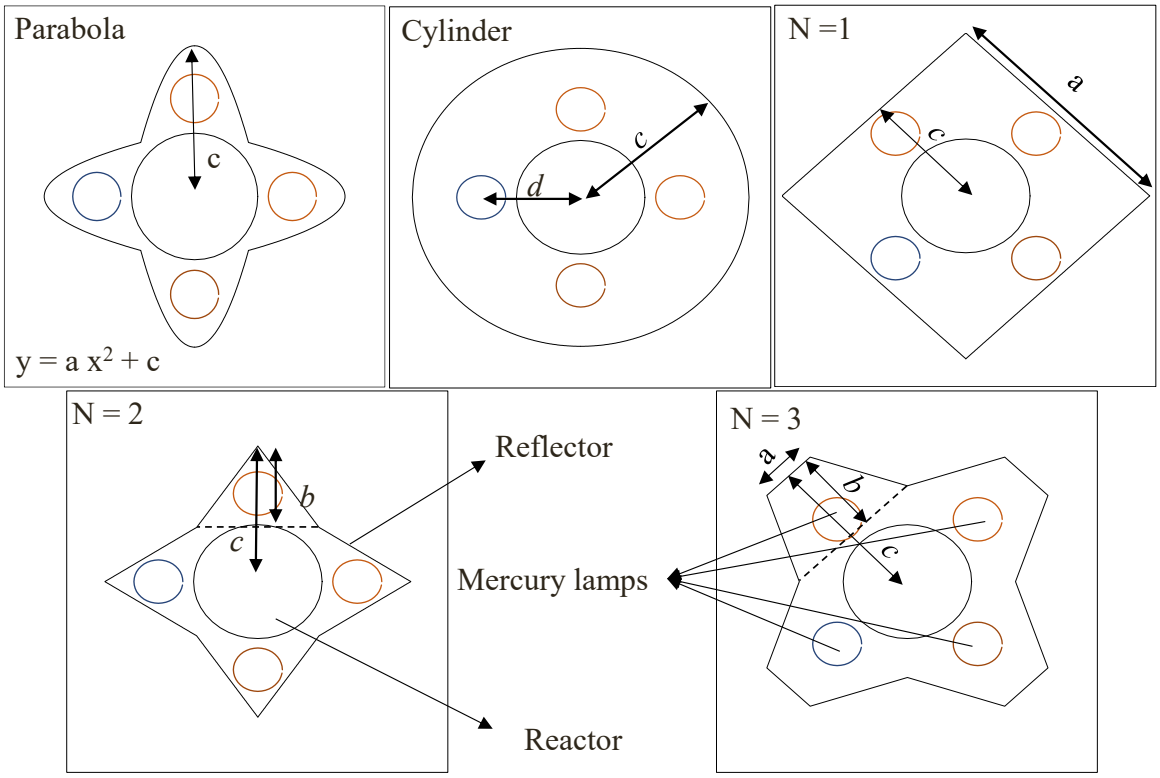

Fig. 2. Parametrization of the geometries simulated by ray tracing.

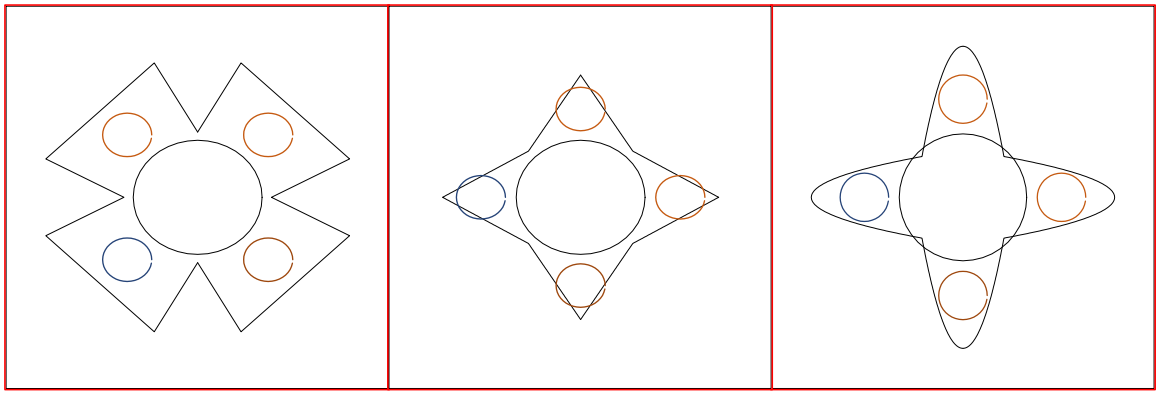

Fig. 3. Example of geometrics discarded for the parametrized simulations.

ions (Fe^{2+}) generated during the irradiation time was experimentally obtained by the slope of Fe^{2+} concentration (mol L^{-1}) as a function of time (s), considering a 25% ferrioxalate degradation, multiplied by actinometric solution volume and Avogadro's number – NA $= 6.02 \times 10^{23}$ mol^{-1}. Radiation power reaching the reactor was calculated using a quantum efficiency at 254 nm of 1.38 [22].

2.3. Ray-tracing calculations

Simulations were carried out using a ray tracing tool based on Microsoft Excel. This tool, originally designed for studying solar radiation in CPC collectors [15,16], has been adapted in this work to calculate the light distribution in closed systems with multiple emission points and reflectors. In all the ray tracing simulations, 4 circular lamps with emissions in all directions were defined. Since the calculations were validated by actinometric measurements, the absorption was considered total, so the rays that reached the reactor were completely absorbed. The reflectance value of the reflective material was also studied and varied depending on the material used. Simulations were also carried out establishing reflectance values of 0 to study the cases in which no reflector was used. The appropriate ray tracing tool for this type of geometry can be found at the following link: https://github.com/PhotonersURJC/Reflectors_RayTracing.

Multiple geometries with different levels of complexity were simulated: Flat one-sided, two-sided, and three-sided geometries, parabolic surfaces, and a cylindrical reflector surrounding the 4 lamps. The parameters established for the configuration of the geometries are shown in Fig. 2, where *c* is the distance between the center of the reactor and the reflector measured at its farthest point, always aligned with the center of the lamp, *b* is the distance between the nearest and farthest point of the reflector and *a* is the width of the side of the reflector furthest from the center of the reactor. For the parabola, *a* is the opening. Finally, *rr* is the radius of the reactor, and *d* is the distance between the center of the reactor and the center of the lamp.

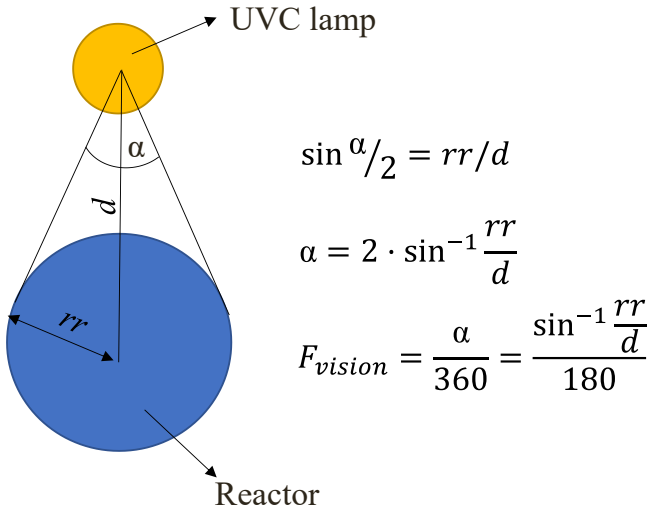

Fig. 4. Geometric calculation of the F_{vision} between the UVC lamps and the photoreactor.

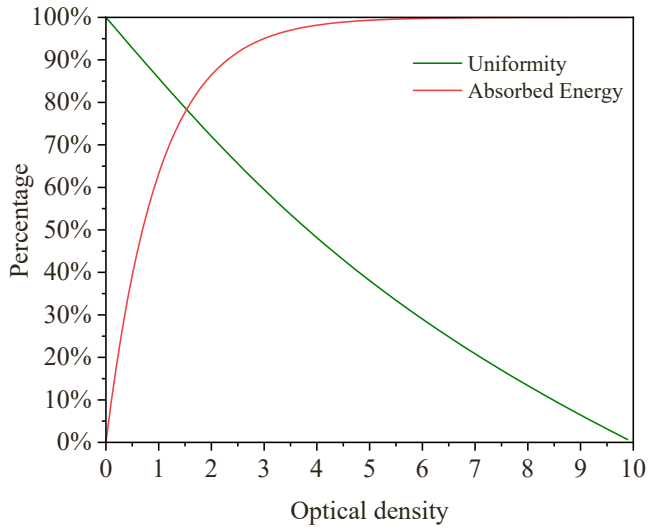

Fig. 5. Absorbed energy and light distribution uniformity as a function of the optical density of the medium.

For the single-sided reflector (N = 1), geometries were studied with side lengths ranging from 2 $\times c_{min}$ (reflector being completely attached to the lamps) to 4 $\times c_{min}$, with an interval of 0.1 cm. For the reflector of N = 2, values of c were studied from c_{min} (value of c in which the vertex of the reflector triangle is attached to the lamps) to 2 $\times c_{min}$ with an interval of 0.2 cm. Values of b were varied between 0.05 and 0.65 cm with an interval of 0.2 cm. For the reflector of N = 3, values of c were studied from c_{min} to 2 $\times c_{min}$ with an interval of 0.2 cm. Values of b were set from 0 to 6.2 cm with an interval of 0.2 cm and values of a between 0 and 4.2 cm with an interval of 0.2 cm. Concerning parabolic reflectors, c values between c_{min} and c_{min}+ 5 $\times rr$ were studied using an interval of 0.2625 cm corresponding to $rr/8$. The values of a ranged from 0 to 3 with an interval of 0.1 cm. In the case of the cylindrical reflector, values of c (corresponding to the radius of the reactor) were studied from c_{min} to 2 $\times c_{min}$.

The ranges studied for each parameter were initially limited considering construction criteria, such as the fact that the reflector should be located outside the lamps. However, the use of the established parameter ranges could still give rise to inconsistent geometries such as those shown in Fig. 3. To rule out these cases and avoid a waste of meaningless computational time, geometric restrictions were established using mathematical rules. All situations created that could give rise to non-possible geometries were excluded.

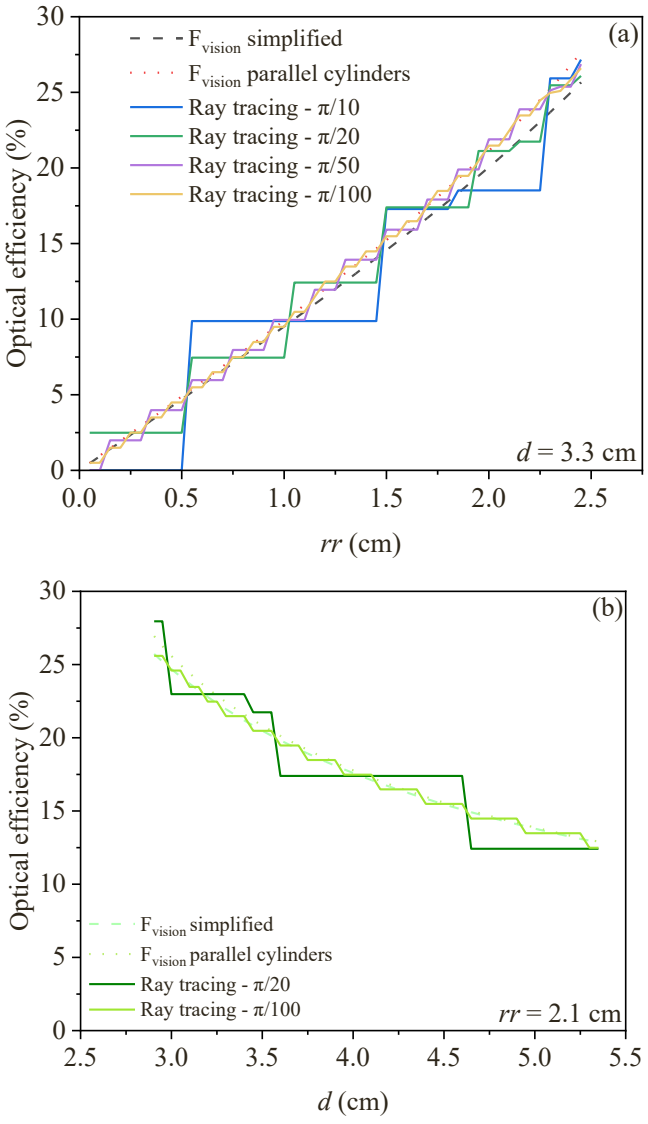

Fig. 6. Optical efficiencies calculated by geometric calculations, parallel cylinder theory, and ray tracing with different numbers of rays for a) different rr values for d = 3.3 cm, and b) different d for rr = 2.1 cm.

3. Results and discussion

3.1. Geometrical design of the reflector

3.1.1. Influence of reactor radius on the radiation distribution

During the design of a photoreactor, any interaction of light with the surrounding elements must be considered, including the non-ideal reflection happening in the reflectors that leads to a loss of the energy available for the reaction. Therefore, it is easy to conclude that the larger the amount of light that goes directly to the reactor from the emission source, the better the energy efficiency.

From geometrical considerations, the vision factor (F_{vision}) between the UVC lamp and the experimentally studied reactor without any reflector can be calculated as the vision factor between parallel cylinders of different radius [23] obtaining a value of 0.22 for rr = 2.1 cm and d = 3.3 cm. On the other hand, if it is assumed that the light source is a line (instead of a cylinder), a simple mathematical expression can be

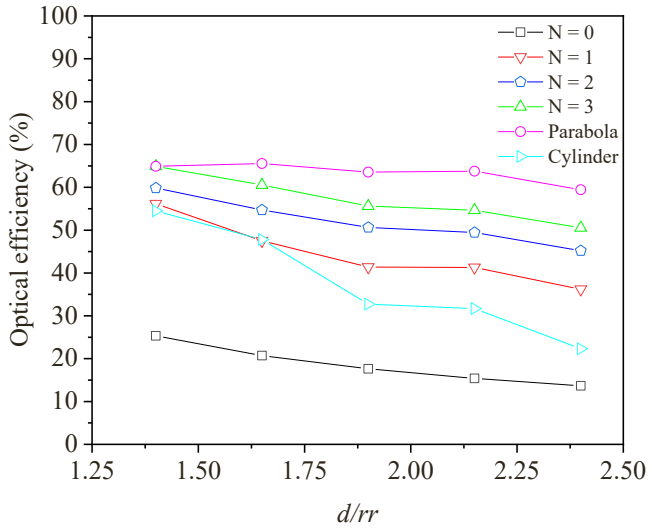

Fig. 7. Optical efficiency for each studied geometry considering different *d/rr* ratios.

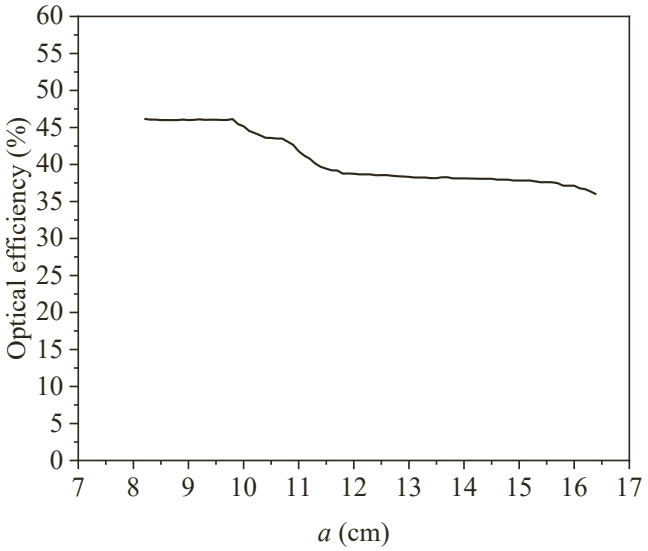

Fig. 8. Optical efficiency for the different reflectors N = 1 in a tube-in-tube reactor for a *d/rr* relation of 1.65.

Table 2
Geometric parameters of the optimal reflectors and optical efficiency for different *d/rr* ratios.

	d/rr	Optical efficiency	*a* (cm)	*b* (cm)	*c* (cm)
N = 0	1.40	25.3%	-	-	-
	1.65	20.7%	-	-	-
	1.90	17.6%	-	-	-
	2.15	15.4%	-	-	-
	2.40	13.7%	-	-	-
N = 1	1.40	56.2%	7.2	-	-
	1.65	47.5%	8.2	-	-
	1.90	41.4%	9.2	-	-
	2.15	41.3%	10.2	-	-
	2.40	36.2%	11.2	-	-
N = 2	1.40	59.8%	-	0.7	3.80
	1.65	54.7%	-	1.8	4.30
	1.90	50.6%	-	2.1	5.00
	2.15	49.5%	-	2.4	5.50
	2.40	45.2%	-	2.7	6.00
N = 3	1.40	64.9%	1.0	1.8	3.60
	1.65	60.5%	0.6	1.6	4.20
	1.90	55.6%	1.0	2.2	5.00
	2.15	54.7%	0.8	2.2	5.40
	2.40	50.6%	0.6	2.4	5.60
Parabola	1.40	64.9%	-0.4	-	4.35
	1.65	65.6%	-0.6	-	4.35
	1.90	63.5%	-0.7	-	4.60
	2.15	63.8%	-0.5	-	5.10
	2.40	59.4%	-0.5	-	5.60
Cylinder	1.40	54.5%	-	-	3.60
	1.65	47.8%	-	-	4.10
	1.90	32.7%	-	-	4.60
	2.15	31.7%	-	-	5.10
	2.40	22.3%	-	-	5.60

obtained (Fig. 4) that also leads to a value of F_{vision} of 0.22 for $rr = 2.1$ cm and $d = 3.3$ cm values, validating the assumption. According to the simplified expression for the calculation of F_{vision}, it is easy to deduce that the amount of direct radiation obtained will be larger the smaller the distance between the reactor and the light source and the higher the radius of the reactor. However, more factors must be considered when choosing the reactor radius. The optical density is defined as the path length (proportional to the radius) multiplied by the absorption coefficient of the medium. In Fig. 5 it can be seen that the increase in optical density causes an increase in the amount of energy absorbed, but also produces a decrease in the uniform distribution of light inside the

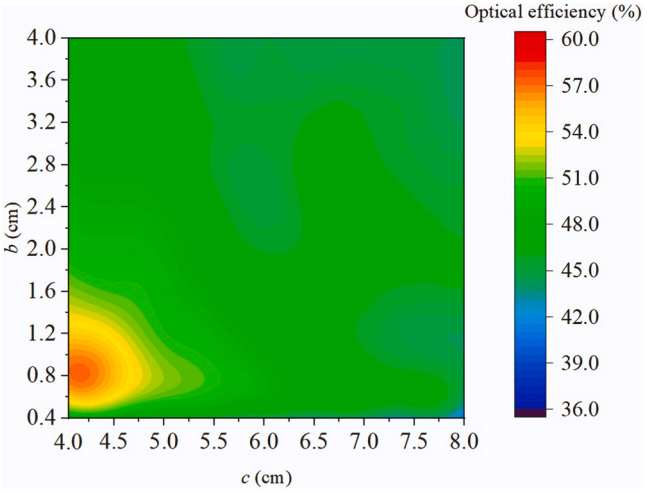

Fig. 9. Optical efficiency for the different reflectors N = 2 in a tube-in-tube reactor for a *d/rr* relation of 1.65.

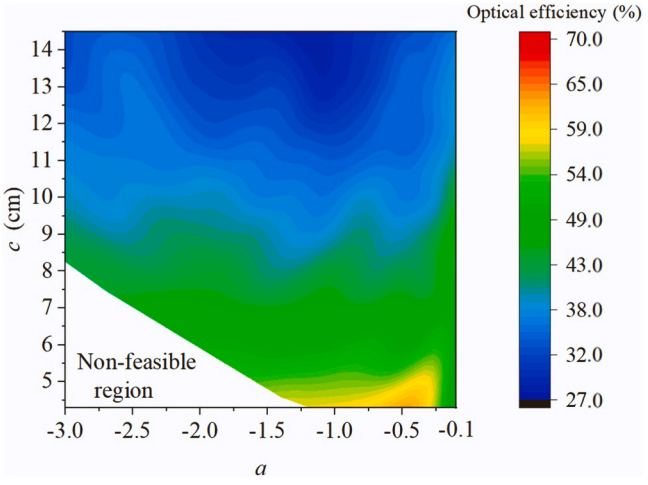

Fig. 10. Optical efficiency for the different parabolic reflectors in a tube-in-tube reactor for a *d/rr* relation of 1.65.

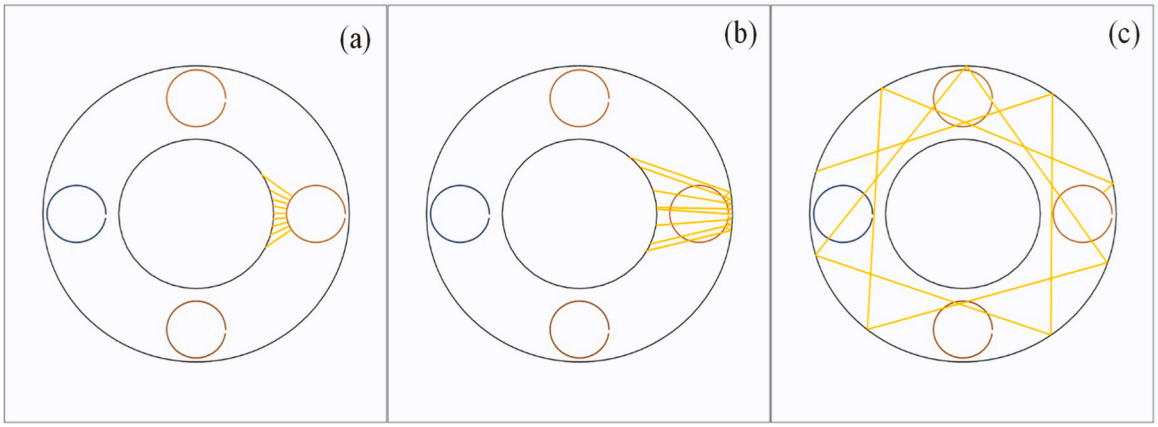

Fig. 11. Ray tracing for cylindrical geometry reflectors for light rays that (a) go directly to the reactor, (b) bounce only once in the reflector, and (c) bounce a large number of times in the reflector.

reactor. Light distribution uniformity, calculated as shown in Eq. (1), is important since low values can produce a decrease in the reaction rate [24] as well as the appearance of dead volumes. Therefore, it is necessary to reach a compromise between absorbed radiation and uniform light distribution, considering this aspect when choosing the radius of the reactor used.

$$\text{Light distribution uniformity} = 1 - \frac{\text{Standart desviation of radiation values}}{\text{Average radiation values}} \quad (1)$$

Making use of the ray tracing tool, it is possible to estimate the optical efficiency of the system, calculated as the ratio between the radiation that reaches the reactor and the radiation emitted by the lamps. The optical efficiency value considers the radiation-reflector interactions, being equivalent to the vision factor when no reflector is used. If the optical efficiency is calculated for $rr = 2.1$ cm and $d = 3.3$ cm and no reflector, a value of 0.22 is obtained, validating the ray tracing tool calculations.

3.1.2. Selection of the number of rays

Fig. 6 shows the vision factor and optical efficiency values calculated for different values of *rr* and *d*. These values were calculated using the three methods presented above and corroborate the good agreement and the conclusions about *d* and *rr* drawn from Fig. 4. In addition, this figure shows optical efficiency values obtained by ray tracing for different spacing distances between rays. This spacing distance is expressed as π/n considering that the result of this operation will be the spacing between each ray within the cylindrical geometry of each lamp. This means that the greater the value of *n*, the greater the number of rays drawn and, therefore, as can be seen in Fig. 6a, the greater precision of the simulation and agreement with the theoretical values. However, it is necessary to consider that high values of *n* increases exponentially the computational cost of the calculation, so it is necessary to reach a compromise. For subsequent simulations, a value of spacing between rays of $\pi/20$ was chosen since the computational time was affordable and the error with respect to the case with higher *n* that can be observed in Fig. 6 with dotted lines was always lower than 5%.

3.1.3. Influence of the d/rr ratio

An essential aspect of the reactor design is the relationship between the distance of the lamps to the reactor center and the radius of the reactor since it affects the amount of direct radiation that reaches the reactor. However, for a correct design, it is also necessary to consider the radiation that bounces in the reflector before reaching the reactor window. For this purpose, simulations of all the cases raised for each geometry were carried out for different *d/rr* ratios. It must be taken into account that if zero absorption of UVC radiation in the air is assumed, the optical efficiency obtained for a given ratio *d/rr* will be constant regardless of the radius of the reactor. Fig. 7 shows the optical efficiency values obtained for the case that reached the highest optical efficiency for each of the studied geometries when using the reflectivity of the anodized aluminum (0.58 for 254 nm).

In all cases, as the value of N increases, the optical efficiency increases. It is also remarkable that, depending on the geometry, the reduction in efficiency of simplified geometries with respect to the parabola is relatively low, confirming the interest in their analysis. On the other hand, an increase in the *d/rr* ratio leads to a decrease in optical efficiency because, as seen above, the closer the lamp is to the reactor window, the greater the amount of direct light that reaches it. This does not happen in parabolic geometry since not only must the proximity of the lamp to the reactor window be considered, but also where the focus of the parabola is located and the position of the lamp with respect to it. In the case of the geometries selected as optimal, as the *d/rr* ratio increased, the lamps were located closer to the focus of the parabola. For this reason, the best case of those studied was the case with a *d/rr* ratio of 1.65, since a compromise was reached between a low *d/rr* ratio but a lower distance to the focus than in the case of the lowest *d/rr*. The results shown in Fig. 7 are very useful since they can be used to design any other tubular reactor with a similar layout in which a specific *d/rr* relationship is defined. The geometric parameters for each optimal reactors are shown in Table 2.

For subsequent simulations, as well as laboratory studies, a *d/rr* ratio of 1.65, was chosen. Even though using a lower ratio gave rise to better results in most of the cases studied, its choice implied very small margins with the outer tube of the photoreactor, so its construction was discarded.

3.1.4. Study of the optimal reflector for a tube-in-tube reactor

This section analyzes in detail the ray tracing simulations carried out for the ratio $d/rr = 1.65$ for reflectors with different geometries of 1, 2, and 3 sides and with cylindrical and parabolic geometries. An optimal reflector of each type was chosen for subsequent experimental validation. In all cases, reflection was considered specular and rays with less than 1% of the initial energy were discarded. Fig. 8 shows the results obtained for $N = 1$. As the size of the reflector sides increases, and therefore the reflector is further away from the lamps and the reactor, a decrease in optical efficiency occurs due to an increase in the number of bounces of light before it reaches the reactor. It can be seen that there is a first zone for this particular reactor where the drop in optical efficiency with the increase on the side of the reactor is very small. The size and fall of this area will vary depending on the geometric arrangement of the reflector. The optimal reflector was the reflector with a minimum *a* of

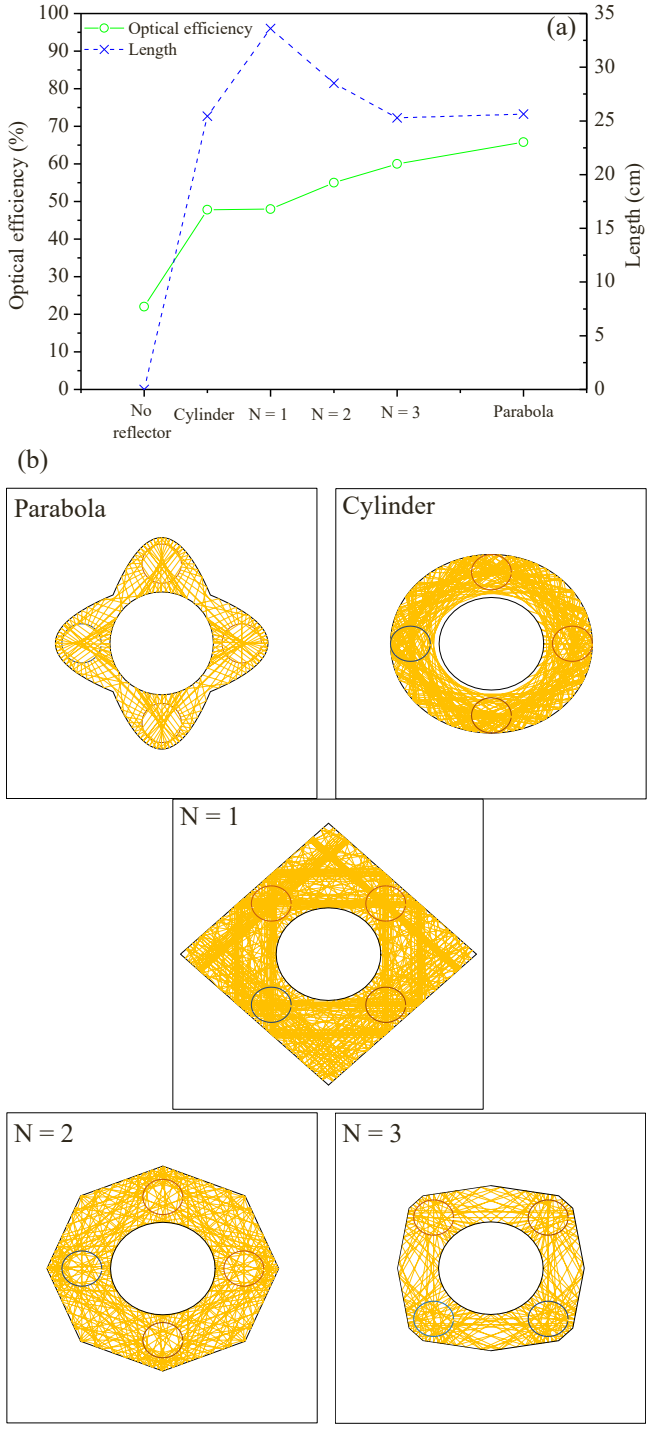

Fig. 12. (a) Optical efficiency values obtained for the optimal reflector geometry for a *d/rr* ratio of 1.65 and (b) ray tracing for each of the optimal reflector geometries.

8.2 cm and an optical efficiency of 46.2%. However, for its subsequent construction for experimental validation and to have a certain margin of error regarding the position of the lamps, it was decided to choose the reflector with a side equal to 8.4 cm and an optical efficiency of 46.1%.

The results for the reflector N = 2 are shown in Fig. 9. Data shows that the optimal optical efficiency values were obtained for the lower *c* values and relatively low *b* values. The optimal reflector among those studied was the reflector with $c = 4.65$ cm and $b = 1.35$ cm, reaching an optical efficiency of 55.8%.

Plotting the results for N = 3 is not straighforward, since they did not

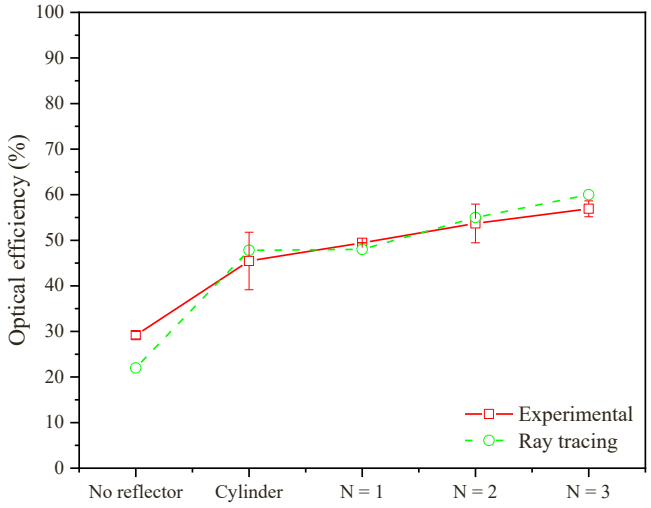

Fig. 13. Comparison of the optical efficiency values experimentally determined by actinometry and the calculations obtained by ray tracing simulations for a *d/rr* ratio of 1.65.

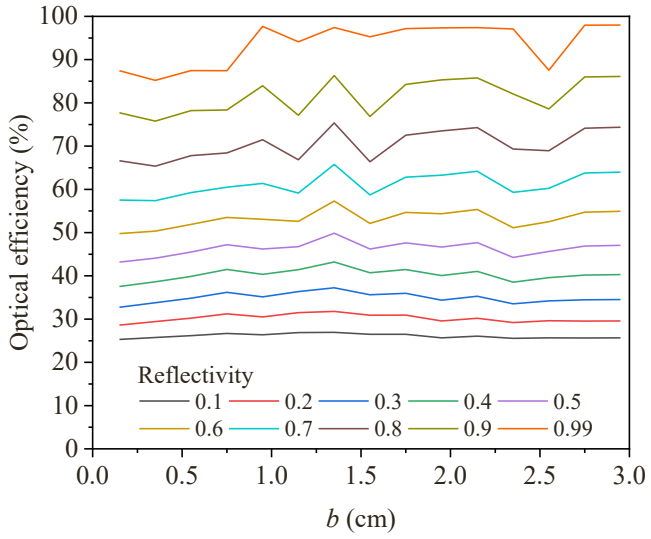

Fig. 14. Optical efficiency values obtained for the case of N = 2 as a function of *b* using a *c* value of 4.65 cm for different reflectivity values and a *d/rr* ratio of 1.65 cm.

allow a clear representation due to the high number of case studies. The data obtained showed how, once again, the geometries that obtained the highest values of optical efficiency were the geometries with low *c* values and the subsequent minimization of the number of bounces. The optimal studied case has values of $c = 4.25$ cm, $b = 1.60$ cm, and $a = 0.80$ cm, resulting in an optical efficiency of 60.0%.

The results obtained for the parabolic reflectors are depicted in Fig. 10. The reflectors that would achieve the highest optical efficiency are those using lower *c* values. In addition, it was observed that the best values of *a* for each value of *c* were related to the position of the lamp and the focus of the parabola. The closer the center of the lamp is to the focus of the parabola, the better the efficiency. The optimal parabolic reflector has values of $c = 4.30$ cm and $a = -0.60$ cm with an optical efficiency of 65.9%.

Regarding the cylindrical reflector, it was observed that the optical efficiency values were constant regardless of the dimensions of the reflector. Most rays bounce a high number of times before reaching the reactor in this geometry (Fig. 11-c), losing all their energy. Therefore,

the radiation that reaches the reflector is only associated with direct radiation (Fig. 11-a) and the low number of rays that reach the reactor after only a single bounce (the rays close to the horizontal and vertical positions with respect to the center of the reactor – Fig. 11-c).

Fig. 12-a shows a summary of the optical efficiency values of the optimal reflectors of each of the proposed geometries as well as the perimeter of the reflector required to build each of them (length of the geometry in two dimensions). The results show that, as the complexity of the reflector increases, the optical efficiency obtained rises, emphasizing that a compromise must be reached between optical efficiency and manufacturing costs. In Fig. 12-b the ray tracing for the optimum reactor of each geometry is shown.

3.2. Ray tracing validation

The simulation predictions were experimentally validated by ferrioxalate actinometry data using the optimal simplified reflectors of ratio $d/rr = 1.65$ fabricated with anodized aluminum. Fig. 13 shows a very good agreement between the optical efficiencies estimated with the simulations and those measured in the laboratory. However, the actinometry result of the reactor without reflector was higher than the theoretically expected value. The major deviation was found in the experiment without reflector, due to minimal but unavoidable reflection existing in the safety cover of the experimental setup.

3.3. Effect of the reflectivity of the material

In the previous sections, all the calculations were carried out using a reflectance value corresponding to anodized aluminum. To get an idea of what would happen using another material, simulations were carried out using reflectance values between 0.1 and 0.99 for a specific example case of the reflector with geometry N = 2 in which the value of c of 4.65 cm was kept fixed and the values of b were varied between 0.15 and 2.95 cm (Fig. 14). The results demonstrated how the trend obtained is similar for the cases of intermediate-high reflectance, with the optimal b value being the same for all of them. When the reflectance is low, the use of one geometry or another is indifferent, because after few bounces in the reflector, all the energy would be lost quickly. Therefore, these results indicated that simulations for different reflector reflectivity would lead to the same optimal geometries as those obtained for anodized aluminum, since the chosen geometries are those that minimize the number of bounces with the reflector.

4. Conclusions

When non-ideal reflector materials are employed, the optimization of the reflector used in a tube-in-tube photoreactor varying lamp-reactor arrangements and reflector geometries with different levels of complexity indicates that, in all cases, the optimum reactor-lamp arrangement is the one that minimizes the lamps distance/reactor radius ratio, since it produces an increase in the direct radiation that reaches the reactor. In addition, it can be concluded that, although parabolic reflectors lead to greater optical efficiency, a geometric simplification using flat surfaces is possible without significant loss of efficiency. Regarding the reflectance of the materials used to manufacture the reflector, it was concluded that the geometry chosen as optimal would be the same for any material, since they are those that minimize the interaction of radiation with the reflector regardless of the material properties.

The proposed analysis and the ray tracing tool developed and made openly available can be applied for the optimal design of any other tubular photoreactor.

CRediT authorship contribution statement

M. Martín-Sómer: Conceptualization, Formal analysis, Investigation, Data curation, Writing – original draft. **J. Moreira**: Investigation, Formal analysis. **Carla Santos**: Investigation. **Ana I. Gomes**: Validation, Writing – review & editing. **J. Moreno-SanSegundo**: Conceptualization, Software. **Vitor J.P. Vilar**: Conceptualization, Validation, Writing – review & editing, Funding acquisition. **J. Marugán**: Validation, Data curation, Writing – review & editing, Funding acquisition.

Declaration of Competing Interest

The authors declare the following financial interests/personal relationships which may be considered as potential competing interests: Vitor J.P Vilar reports financial support was provided by Fundação para a Ciência e a Tecnologia.

Data availability

The link of the ray tracing told is shared in the manuscript.

Acknowledgments

The authors gratefully acknowledge the financial support of the Spanish State Research Agency (AEI) and the Spanish Ministry of Science and Innovation through the project AQUAENAGRI (PID2021-126400OB-C32) and Comunidad de Madrid through the program REMTAVARES (P2018/EMT-4341). This work was also financially supported by LA/P/0045/2020 (ALiCE), UIDB/50020/2020 and UIDP/50020/2020 (LSRE-LCM), funded by national funds through FCT/MCTES (PIDDAC). The authors would like to thank the EU and Bundesministerium für Bildung und Forschung, Germany, Ministero dell'Università e della Ricerca, Italy, Agencia Estatal de Investigación, Spain, Fundação para a Ciência e a Tecnologia, Portugal, Norges forskningsråd, Norway, Water Research Commission, South Africa for funding, in the frame of the collaborative international consortium SERPIC financed under the ERA-NET AquaticPollutants Joint Transnational Call (GA No. 869178). This ERA-NET is an integral part of the activities developed by the Water, Oceans and AMR Joint Programming Initiatives. Miguel Martín-Sómer also acknowledges Spanish MEFP for his Jose Castillejo grant (CAS21/00014).

References

[1] J.P. Ghosh, R. Sui, C.H. Langford, G. Achari, C.P. Berlinguette, A comparison of several nanoscale photocatalysts in the degradation of a common pollutant using LEDs and conventional UV light, Water Res. 43 (2009) 4499–4506, https://doi.org/10.1016/j.watres.2009.07.027.

[2] C. Minero, D. Vione, A quantitative evalution of the photocatalytic performance of TiO2 slurries, Appl. Catal. B Environ. 67 (2006) 257–269, https://doi.org/10.1016/j.apcatb.2006.05.011.

[3] A.C. Chevremont, J.L. Boudenne, B. Coulomb, A.M. Farnet, Fate of Carbamazepine and Anthracene in Soils Watered with UV-LED Treated Wastewaters, 47, 2013, pp. 6574–6584. ⟨https://doi.org/10.1016/j.watres.2013.08.031⟩).

[4] K. Song, M. Mohseni, F. Taghipour, Application of ultraviolet light-emitting diodes (UV-LEDs) for water disinfection: a review, Water Res. 94 (2016) 341–349, https://doi.org/10.1016/j.watres.2016.03.003.

[5] M.A.S. Ibrahim, J. MacAdam, O. Autin, B. Jefferson, Evaluating the impact of LED bulb development on the economic viability of ultraviolet technology for disinfection, Environ. Technol. 35 (2014) 400–406, https://doi.org/10.1080/09593330.2013.829858.

[6] M.A. Wü Rtele, T. Kolbe, M. Lipsz, A. Kü Lberg, M. Weyers, M. Kneissl, M. Jekel, Application of GaN-based ultraviolet-C light emitting diodes e UV LEDs e for water disinfection, Water Res. 45 (2011) 1481–1489, https://doi.org/10.1016/j.watres.2010.11.015.

[7] M. Keshavarzfathy, F. Taghipour, Radiation modeling of ultraviolet light-emitting diode (UV-LED) for water treatment, J. Photochem. Photobiol. A Chem. 377 (2019) 58–66, https://doi.org/10.1016/j.jphotochem.2019.03.030.

[8] V. Pareek, S. Chong, M. Tadé, A.A. Adesina, Light intensity distribution in heterogenous photocatalytic reactors, Asia-Pac. J. Chem. Eng. 3 (2008) 171–201, https://doi.org/10.1002/APJ.129.

[9] Á. García-Gil, C. Casado, C. Pablos, J. Marugán, Novel procedure for the numerical simulation of solar water disinfection processes in flow reactors, Chem. Eng. J. 376 (2019), 120194, https://doi.org/10.1016/j.cej.2018.10.131.

[10] C. Casado, Á. García-Gil, R. van Grieken, J. Marugán, Critical role of the light spectrum on the simulation of solar photocatalytic reactors, Appl. Catal. B Environ. 252 (2019) 1–9, https://doi.org/10.1016/j.apcatb.2019.04.004.
[11] Z. Wang, J. Liu, Y. Dai, W. Dong, S. Zhang, J. Chen, CFD modeling of a UV-LED photocatalytic odor abatement process in a continuous reactor, J. Hazard. Mater. 215–216 (2012) 25–31, https://doi.org/10.1016/j.jhazmat.2012.02.021.
[12] M. Keshavarzfathy, F. Taghipour, Computational modeling of ultraviolet light-emitting diode (UV-LED) reactor for water treatment, Water Res. 166 (2019), 115022, https://doi.org/10.1016/j.watres.2019.115022.
[13] J. Moreno, C. Casado, J. Marugán, Improved discrete ordinate method for accurate simulation radiation transport using solar and LED light sources, Chem. Eng. Sci., 205, 2019, pp. 151–164. (Accessed July 11, 2019).
[14] J. Moreno-SanSegundo, C. Casado, J. Marugán, Enhanced numerical simulation of photocatalytic reactors with an improved solver for the radiative transfer equation, Chem. Eng. J. 388 (2020), 124183, https://doi.org/10.1016/j.cej.2020.124183.
[15] J. Moreno-SanSegundo, M. Martín-Sómer, J. Marugán, Dynamic concentration factor: a novel parameter for the rigorous evaluation of solar compound parabolic collectors, Chem. Eng. J. 437 (2022), 135360, https://doi.org/10.1016/J.CEJ.2022.135360.
[16] J. Moreno-SanSegundo, M. Martín-Sómer, Javier Marugán, Ray Tracing Tool, 2021.
[17] E.C. Lumbaque, D.S. Lüdtke, D.D. Dionysiou, V.J.P. Vilar, C. Sirtori, Tube-in-tube membrane photoreactor as a new technology to boost sulfate radical advanced oxidation processes, Water Res. 191 (2021), 116815, https://doi.org/10.1016/J.WATRES.2021.116815.
[18] P.H. Presumido, R. Montes, J.B. Quintana, R. Rodil, M. Feliciano, G.L. Puma, A. I. Gomes, V.J.P. Vilar, Ozone membrane contactor to intensify gas/liquid mass transfer and contaminants of emerging concern oxidation, J. Environ. Chem. Eng. 10 (2022), 108671, https://doi.org/10.1016/J.JECE.2022.108671.
[19] V.J.P. Vilar, P. Alfonso-Muniozguren, J.P. Monteiro, J. Lee, S.M. Miranda, R.A. R. Boaventura, Tube-in-tube membrane microreactor for photochemical UVC/H2O2 processes: a proof of concept, Chem. Eng. J. 379 (2020), 122341, https://doi.org/10.1016/J.CEJ.2019.122341.
[20] A.I. Gomes, T.F.C.V. Silva, M.A. Duarte, R.A.R. Boaventura, V.J.P. Vilar, Cost-effective solar collector to promote photo-Fenton reactions: a case study on the treatment of urban mature leachate, J. Clean. Prod. 199 (2018) 369–382, https://doi.org/10.1016/J.JCLEPRO.2018.07.113.
[21] F.C. Moreira, E. Bocos, A.G.F. Faria, J.B.L. Pereira, C.P. Fonte, R.J. Santos, J.C. B. Lopes, M.M. Dias, M.A. Sanromán, M. Pazos, R.A.R. Boaventura, V.J.P. Vilar, Selecting the best piping arrangement for scaling-up an annular channel reactor: an experimental and computational fluid dynamics study, Sci. Total Environ. 667 (2019) 821–832, https://doi.org/10.1016/J.SCITOTENV.2019.02.260.
[22] J.R. Bolton, M.I. Stefan, P.S. Shaw, K.R. Lykke, Determination of the quantum yields of the potassium ferrioxalate and potassium iodide–iodate actinometers and a method for the calibration of radiometer detectors, J. Photochem. Photobiol. A Chem. 222 (2011) 166–169, https://doi.org/10.1016/J.JPHOTOCHEM.2011.05.017.
[23] Y.A. Cengel, S. Klein, W. Beckman. Heat Transfer: A Practical Approach, WBC McGraw-Hill, Boston, 1998.
[24] M. Martín-Sómer, C. Pablos, R. van Grieken, J. Marugán, Influence of light distribution on the performance of photocatalytic reactors: LED vs mercury lamps, Appl. Catal. B Environ. 215 (2017) 1–7, https://doi.org/10.1016/j.apcatb.2017.05.048.